PHYSICAL REVIEW B VOLUME 24, NUMBER 8 15 OCTOBER 1981

Tellurium donors in silicon

H.G. Grimmeiss and E. Janzén
Department of Solid State Physics, University of Lund, Box 725, S-220 07 Lund, Sweden

H. Ennen, O. Schirmer, J. Schneider, and R. Wörner
Institut für Angewandte Festkörperphysik, Fraunhofer Gesellschaft, Eckerstrasse 4, D-78 Freiburg, Federal Republic of Germany

C. Holm and E. Sirtl
Heliotronic GmbH, P.O. Box 1129, D-8263 Burghausen, Federal Republic of Germany

P. Wagner
Max-Planck-Institut für Festkörperforschung, Heisenbergstrasse 1, D-7 Stuttgart, Federal Republic of Germany

(Received 23 April 1981)

The electronic properties of chalcogens as dopants in silicon are discussed with emphasis on tellurium. Tellurium gives rise to two dominant donor levels which have been studied by junction space-charge techniques, infrared absorption, and ESR. Both donor levels exhibit excited states (Rydberg series and multivalley split-off states) which are in agreement with those expected for singly and doubly charged centers, respectively. These results suggest that tellurium causes a double donor level in silicon. One of the donor states has been identified by ESR as Te^+. Hyperfine interactions with the $I=\frac{1}{2}$ nuclei ^{125}Te and ^{123}Te as well as with ^{29}Si in the surrounding lattice have been observed. The ESR line shape due to the interaction with ^{29}Si suggests that the tellurium donor levels occupy substitutional sites. Photo-ESR clearly shows that both the ESR signal and the data obtained from junction space-charge techniques and infrared absorption measurements originate from the same center. From the excited states, temperature-independent ground-state binding energies of 198.8 and 410.8 meV, respectively, have been deduced.

I. INTRODUCTION

If an atom of the host lattice in silicon is replaced by an atom belonging to the fifth group in the Periodic Table, the potential binding the extra electron at the impurity atom can in most cases be approximated by a hydrogenlike potential.[1] This gives rise not only to an energy level in the band gap for the impurity ground state but, in addition, also to a series of excited states. In silicon, the ground-state energies of these impurities are of the order of 50 meV. Such centers are therefore called "shallow" impurities and are widely used in semiconductor technology for modifying the type and degree of electrical conductivity. The energy levels of the excited states are almost independent of the ground-state energies and are well described by effective-mass theory.[2–4]

If, on the other hand, a host atom in silicon is replaced by an atom from the sixth group in the Periodic Table, two extra electrons are available which may give rise to double donors. The potential binding these two electrons at the impurity atoms is frequently compared with that for the two electrons in a helium atom.[5] The ground states of impurity atoms from the sixth group which have been investigated so far lie at much greater distances from the conduction band than shallow impurity levels, thus creating so-called "deep" impurity levels. Apart from some transition metals, the excitation and recombination spectra of deep centers in semiconductors generally show a smooth energy dependence without any of the detailed structure which is otherwise characteristic of shallow centers. This has often been considered as an indication for the nonexistence of excited states at deep centers. Recently, however, evidence was given that the electronic properties of certain sulfur- and selenium-related deep donors in silicon are best understood in terms of excited states.[6–8]

It could be shown that two types of excited states are involved: those which are generally referred to as the Rydberg series and those which originate from the multivalley nature of the conduction band. Two of the donor states investigated were midgap levels and, hence, represent the deepest energy levels which can be created in silicon.

Since the doping with chalcogens was performed at relatively low temperatures,[9] only two dominant donor levels were observed in Si:S (Ref. 7) and Si:Se (Ref. 6). Whereas the midgap levels in Si:S and Si:Se (the *A* centers) have the "thermal activation energies" of 0.59 and 0.52 eV, respectively, the corresponding binding energies of the shallower energy levels (the *B* centers) are $E_c - 0.32$ eV and $E_c - 0.30$ eV. In all cases very large electron-capture cross sections have been observed. This we believe is due to the excited states. The data obtained from the *B* centers strongly suggest that the electron-capture process is at least partly governed by a cascade process.[6,7]

Unlike sulfur and selenium, tellurium has not so far attracted much interest. In spite of the fact that tellurium often has been used for ion implantation in silicon, very little information about the electronic properties of tellurium-doped silicon is available in the literature.[10–18] Rather peculiar properties of the energy levels observed in tellurium-implanted silicon have been reported.[12] These may result from residual implantation damage effects. On the other hand, several authors claim that most of the implanted tellurium atoms are incorporated on substitutional sites.[12–17] It will be shown later that these results are in agreement with our own data. As early as 1963, Fischler used vapor-transport processes to introduce tellurium into silicon.[18] From Hall-effect measurements, he found an energy level due to tellurium doping 0.14 eV below the conduction band.

One of the major problems encountered in the investigation of deep energy levels is that of the chemical identification of the defect studied. In a recent paper, the diffusion[19] profile of selenium in silicon was investigated using secondary-ion mass spectroscopy (SIMS) and two different junction space-charge techniques. In both cases, similar profiles were obtained. Since the profiles measured by SIMS were due to selenium atoms, it was concluded that the two dominant donor levels previously investigated[6,8] in Si:Se by junction space-charge techniques are in fact selenium related. From these measurements, however, no information about the local environment of the selenium atoms could be obtained.

The purpose of this paper is to present a thorough study of tellurium-doped silicon and to give further evidence for the identification of the energy levels in selenium-doped silicon previously investigated. Using these new experimental data, a discussion of the electronic properties of chalcogen-doped silicon is given. The data in Si:Te have been obtained using three entirely different measuring techniques, viz., infrared absorption, ESR (including photo-ESR), and junction space-charge techniques. The results obtained show that the energy levels studied in Si:Te are probably caused by single substitutional tellurium atoms. The similarity of the observations made with Si:Se and Si:S (Refs. 6–8) suggests the same microscopic model also for these elements. This implies that the data presented in this paper and previous papers[6–8] are best understood if the *A* centers are identified with Te^+, Se^+, and S^+, respectively, and the *B* centers with Te^0, Se^0, and S^0.

II. EXPERIMENTAL DETAILS

A. Sample preparation

The samples used in this paper have been prepared with two different techniques giving identical results. Those prepared at Wacker (vapor transport) were used for infrared-absorption and ESR measurements. They were also used together with the samples prepared at the University of Lund (diffusion) for measurements employing junction space-charge techniques.

The original purpose of all the preparative work on this subject at Wacker was the desire to learn more about the inherent properties of sulfur in silicon. The investigations were soon extended to selenium and tellurium—for the simple reason that certain properties of the materials could better be understood from a knowledge of their variation within a homogeneously group of elements incorporated by one and the same method during crystal growth.

For preparing homogeneously doped samples, a modification of a close-spaced chemical transport method via the gaseous state[20,21] was developed. This will be described elsewhere.[22] In our case, vapor-transport agents are group-VI elements only. The experimental setup used for growing epitaxial silicon specimens is shown in Fig. 1.

In contact with the silicon seed and source material volatile silicon chalcogenides are formed at

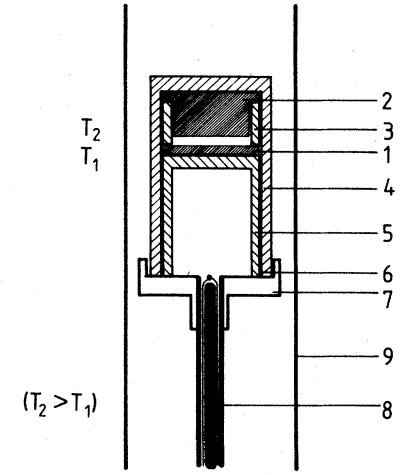

FIG. 1. Experimental setup for high-temperature vapor growth of extra-large epitaxial layers of chalcogen-doped silicon. 1—Si substrate (seed), 2—Si source, 3—quartz ring (spacer), 4—quartz "beaker," external, 5—quartz "beaker," internal, 6—quartz seal (ring-shaped welding), 7—support for ampoule system (alumina + quartz), 8—thermocouple, 9—furnace tube.

high temperatures. In a shallow thermal gradient, epitaxial silicon layers are deposited under quasi-equilibrium conditions in which the chalcogen is incorporated at its maximum solubility value. Moreover, doping through crystal growth occurs without additional lattice defects being generated, as is known from the application of indiffusion methods.

Electronic-grade float-zoned silicon monocrystals of differently doped qualities (Wacker-Chemitronic) were used as source and substrate specimens (see Fig. 1). For the material discussed in this article, 59-grade selenium (Balzers) and 69-grade tellurium (Cominco), respectively, provided the vapor-transport vehicle. Epitaxial overgrowth was accomplished at geometrical dimensions of 30-mm diameter maximum and thicknesses up to 10 mm (for Te-doped silicon at maximum growth rates of 0.3 μm min^{-1}).

The Si:Te diodes prepared at the University of Lund were fabricated on 7-Ω cm n-type silicon by diffusion using conventional technology. The samples were tellurium diffused at 1200° C for 4 h in a sealed evacuated quartz ampoule to give samples with a concentration of tellurium-related centers of 2×10^{15} cm^{-3}. In order to minimize erosion of the samples during diffusion, the tellurium was mixed with silicon powder. The p^+n junctions and Schottky contacts were fabricated in the conventional manner.

B. Experimental techniques

Three completely different experimental techniques were used for investigating our samples: junction space-charge techniques,[23] absorption measurements, and ESR studies. The samples were investigated using various forms of junction techniques. These include isothermal capacitance, deep-level transient spectroscopy (DLTS), admittance spectroscopy, photocapacitance, dark capacitance, and dark current transient techniques. Isothermal capacitance and photocapacitance measurements were performed at either constant capacitance[24] or constant voltage. The spectral sensitivity of these techniques in the threshold region could greatly be increased by using the initial-slope technique described in detail in a previous paper.[8]

Absolute photoionization cross sections σ^0 were calculated from the measured optical emission rates e^o and photon fluxes ϕ using the relation[25] $\sigma^0=e^o/\phi$. Because of the large differences in sensitivity for intrinsic and extrinsic optical excitations, any stray light had to be very carefully excluded during the experiments. Globar or incandescent lamps with either a Zeiss MM3 prism double monochromator or a double-grating monochromator from Jarrel Ash or Jobin Yvon (HRD 1) were therefore used as light sources. For further suppression of stray light, various sets of filters were employed.

The low-temperature infrared-absorption spectra were recorded on either a grating Perkin-Elmer 180 or Fourier-Nicolet MXI spectrometer. In addition, a Spex grating monochromator system was used for wavelengths shorter than 3.5 μm.

The ESR studies were performed on a Bruker ER 420 X band spectrometer at 20 K. The light dependence of the ESR intensity was measured by focusing a 150-W halogen lamp through the slotted front of the ESR cavity onto the sample, the light having been monochromatized by either a set of interference filters or a grating monochromator. Relative calibration of the photon flux was accomplished using a thermopile. By replacing the sample in the cavity by a calibrated solar cell absolute values of the photon flux could be obtained.

III. THEORETICAL BACKGROUND

Relevant parts of the theory involved in our experiments will be treated later, together with the experimental results. Only two features of more general importance will be discussed in this section.

The ground state of a donor level in silicon which is mainly built up from conduction-band states is expected to split up because of the multivalley nature of the conduction band.[26] For a donor level with T_d symmetry, the sixfold-degenerate 1*s* "ground" state is split into a one fold-degenerate $1sA_1$, a threefold-degenerate $1sT_2$ and a twofold-degenerate $1sE$ state (cf. Fig. 2). In addition, the Coulombic tail of the impurity potential gives rise to a set of excited states commonly referred to as the Rydberg series.

Recently, a model for two-stage thermal emission and capture processes was proposed by Gibb *et al.*[27] (Fig. 3). In this model, the electron is first excited thermally from the ground state to the deepest excited state accessible in a cascade capture process. For chalcogens in silicon, this state may be the $2p_0$ state. It is assumed to lie at an energy E_2 above the ground state. The thermal emission of electrons from this state into the conduction band competes with the recapture of charge carriers into the ground state. At higher temperatures ($e_1 >> \nu_2$), the thermal emission rate for electrons, e_n^t, can be expressed as

$$e_n^t = \nu_2 \exp(-E_2/kT)$$
$$= \nu_0 \exp[-(E_2+E_a)/kT], \quad (1)$$

where E_a is the thermal activation energy of the recapture process. E_a is zero if, for example, the recapture of the electron is radiative. For emission processes governed by Eq. (1), an Arrhenius plot of the thermal emission rate should therefore yield an activation energy which is given by E_2+E_a.

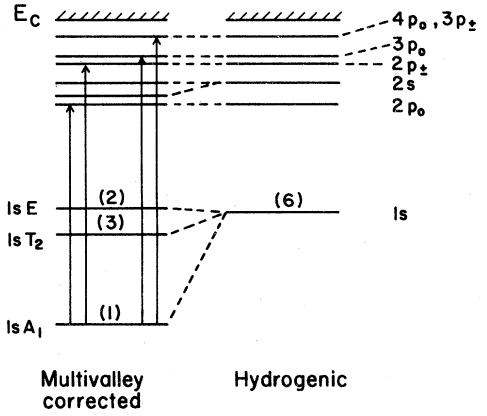

FIG. 2. Energy-level scheme of a donor in silicon taking the multivalley nature of the conduction band into account.

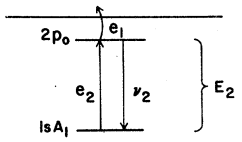

FIG. 3 Emission via an excited state according to Ref. 27.

IV. EXPERIMENTAL RESULTS

A. Junction space-charge techniques and infrared absorption in Si:Te

A typical DLTS (Ref. 28) spectrum for one of our tellurium-diffused Schottky diodes is shown in Fig. 4. Similar spectra were obtained for vapor-transported samples. For comparison the spectrum of a reference sample fabricated in exactly the same way as the Si:Te samples but without the addition of tellurium is also shown. It is readily seen that doping with tellurium gives rise to two dominant energy levels, the deep *A* center and the shallower *B* center.

The logarithms of the thermal emission rates[25] for electrons versus $1/T$ (Arrhenius plots) for the two centers are shown in Fig. 5. It should be mentioned that the transients were slightly nonexponential, probably due to electric field effects.

1. The shallower donor level (B center) in Si:Te

From the data presented in Fig. 5, an activation energy of 196 meV is obtained for the *B* center in Si:Te. To facilitate the interpretation of this value, infrared absorption measurements were performed

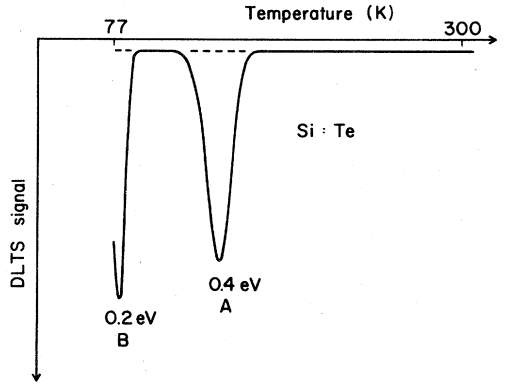

FIG. 4. DLTS spectra of tellurium-doped Schottky diodes (solid curve) and of reference diodes not deliberately doped with tellurium (dashed curve).

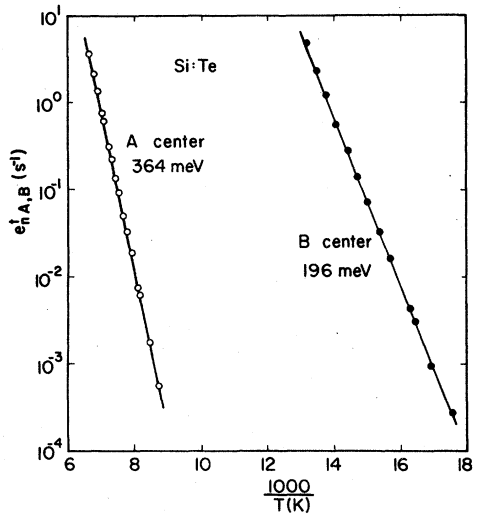

FIG. 5. Arrhenius plots of the thermal emission rates of electrons for the two dominating donor levels in tellurium-doped silicon.

on tellurium-doped n-type samples.

Overall transmission spectra, covering the spectral range from 4000 to 1000 cm^{-1}, are shown in Fig. 6 for n-type and weakly n-type Si:Te samples. For both samples, traces of interstitial oxygen could be detected by the characteristic local-vibrational modes at 1205 cm^{-1} (149.4 meV) and 1136 cm^{-1} (140.8 meV).[29]

The lower spectrum of Fig. 6 was recorded on an n-type 0.19-Ω cm tellurium-doped silicon sample. The occupancy of the B center, i.e., the neutral charge state of the tellurium impurity, Te^0, is stabilized in this sample by the Fermi level. Starting at low energies, the first line due to excitation of the electron from the B center is seen at 1288 cm^{-1} (159.7 meV): this is shown on an expanded scale in Fig. 7. The line at 1288 cm^{-1} arises from the electric-dipole ($E1$) allowed transition $1sA_1 \rightarrow 1sT_2$. A slight asymmetry of the line might be explained by the $E1$-forbidden transition, $1sA_1 \rightarrow 1sE$. This transition may borrow oscillator strength from the nearby $E1$-allowed transition via random electric fields in the crystal. The line at 1217 cm^{-1} (151 meV) is probably due to oxygen although the relative strength of absorption for the two lines 1217 and 1205 cm^{-1} should be different at 5 K.[30]

Shortly before the photoionization of electrons directly into the conduction band at photon energies of about 0.2 eV, two sharp absorption lines are observed at 187.3 and 192.4 meV (Fig. 8). These are due to transitions from the deep $1sA_1$ ground state into the shallow Rydberg levels $2p_0$ and $2p_\pm$,

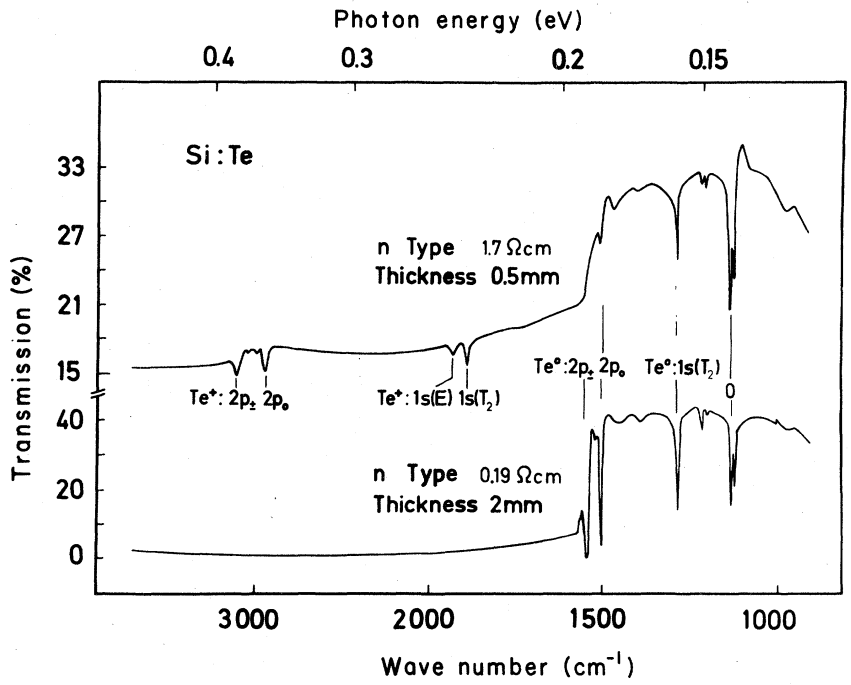

FIG. 6. Overall transmission spectra of n-type (0.19 Ω cm, lower trace) and weakly n-type Si:Te samples (upper trace) at $T \cong 20$ K.

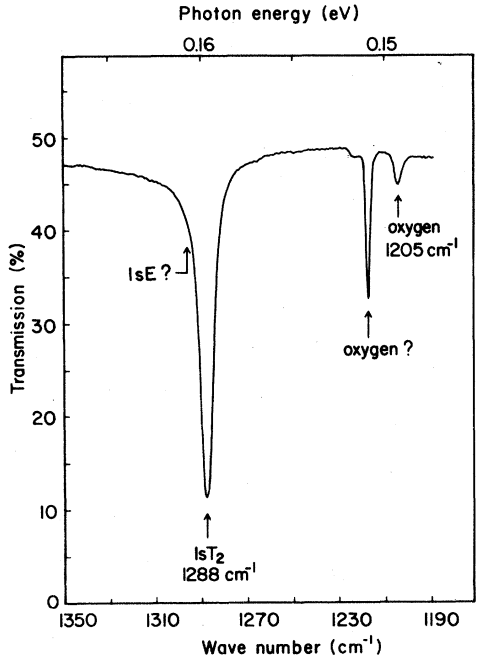

FIG. 7. Lowest-energy electron excitations, $1sA_1 \rightarrow 1sT_2$, $1sE$ of Te^0 donor states in silicon. The highest energy (1205 cm^{-1}) local mode of interstitial oxygen is also detected. The origin of the line at 1217 cm^{-1} is uncertain but is probably also due to oxygen. $T \leq 5$ K.

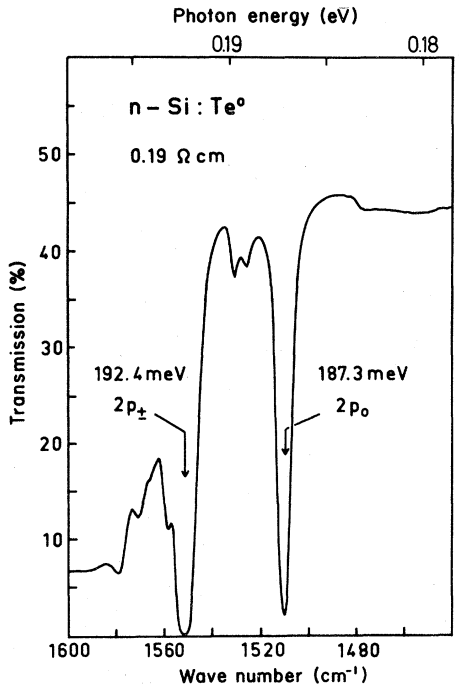

FIG. 8. $1sA_1 \rightarrow 2p_0$ and $1sA_1 \rightarrow 2p_\pm$ absorption lines of Te^0 in silicon at $T \leq 5$ K.

respectively. The energy separation for these two lines of 5.1 meV is in agreement with the value of 5.11 meV deduced from effective-mass theory (EMT).[4] The EMT value for the energy separation of the $2p_\pm$ level form the conduction band is 6.40 meV. Hence, the binding energy of the B center $[E_c - E_T(Te^0)]$ is 198.8 meV.

Comparing the results from our absorption measurements with data obtained from measurements of the thermal emission rate, it is quite obvious that E_a cannot be equal to zero. From the data presented in Fig. 5, an activation energy and, hence, a value of 196 meV for $E_2 + E_a$ was obtained. Our absorption measurements show that the energy separation between the $2p_0$ state and the ground state (i.e., E_2) is 187.3 meV. Assuming that the two-stage emission (via the $2p_0$ state) model is valid E_a would then be equal to about 9 meV, implying that the transition $2p_0 \rightarrow 1sA_1$ is nonradiative. This would not be surprising, since E_2 is equivalent to only three optical-phonon energies. The capture of the electrons from the conduction band into the B center was too fast to be measured with our equipment. Unlike Si:S (Ref. 7) and Si:Se (Ref. 6), the thermal activation energy of the electron-capture process could therefore not be determined and no further evidence to facilitate the interpretation of our absorption data can be given. In the two-state model the activation energy of the capture process is namely equal to the difference between the energy spacing of the conduction band from the the lowest state accessible in a cascade process (e.g., $2p_0$) and E_a.

2. *The deeper donor level (A center) in Si:Te*

Since the Fermi level of the weakly n-type Si:Te sample (cf. Fig. 6) is relatively low, some of the B centers are already empty at thermal equilibrium. If the A and B centers are different charge states of a double donor, the empty B centers represent singly ionized tellurium centers, Te^+, and, hence, filled A centers. It is expected that the excitation of electrons from the A centers occurs at higher energies than for the B centers (cf. Fig. 2). The energy spacing between the transition $1sA_1 \rightarrow 1sT_2$ at 234.2 meV and the transition $1sA_1 \rightarrow 1sE$ at 239.6 meV is more pronounced for the A center than for the B center. Prior to the photoionization threshold, sharp absorption lines are observed at 364.4 and 385.2 meV due to the excitation into the Rydberg states $2p_0$ and $2p_\pm$, respectively (Fig. 9). The ener-

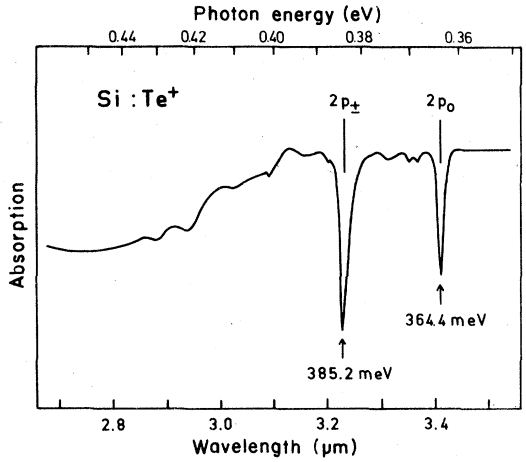

FIG. 9. $1sA_1 \rightarrow 2p_0$ and $1sA_1 \rightarrow 2p_\pm$ absorption lines of Te^+ in silicon at $T=5$ K.

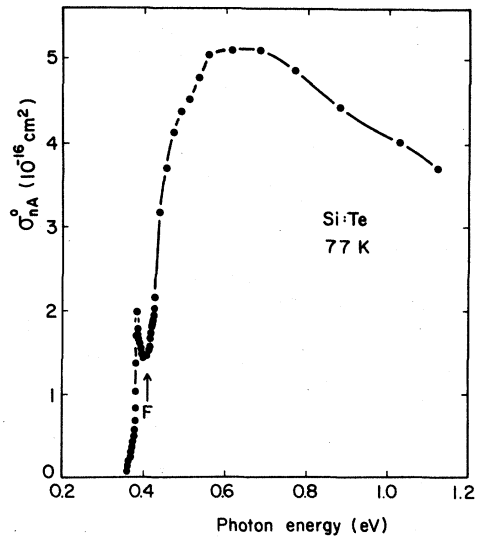

FIG. 10. Spectral dependence of the photoionization cross section of electrons for the A center plotted in a linear scale. The onset of photoexcitation of electrons from the ground state directly into the conduction band is marked with an arrow (F). The structure at lower energies is due to photothermal ionization processes.

gy spacing of 20.8 meV between these two lines agrees with the EMT value for an ionized double donor which should be four times 5.11 meV, i.e., 20.44 meV. The binding energy of the A center at 5 K is obtained by adding the EMT value of 4 (6.40) = 25.6 meV to the energy of the $2p_\pm$ state, giving a value of 410.8 meV.

Using junction space-charge techniques[23,25] information about these excitation energies can be obtained at much higher temperatures by measuring the spectral distribution of photoionization cross sections. Figure 10 shows a linear plot of the spectrum of the photoionization cross secton for electrons σ^0_{nA} for the A center at 77 K. The rapid increase of σ^0_{nA} with increasing energy, starting at about 411 meV (as indicated by the arrow F), is caused by the photoexcitation of electrons from the ground state directly into the conduction band. The structures seen at energies smaller than that indicated by the arrow F are due to internal transitions from the ground state into excited states. Internal transitions are expected to cause changes in the diode capacitance only if they originate from a two-step photothermal excitation process in which the electron is first excited optically from the ground state into an excited state and then further excited into the conduction band by absorbing one or several phonons. Expanding this region of the 77 K spectrum (cf. insert of Fig. 11), three clearly resolved peaks can be distinguished. Figure 11 shows the same data in a logarithmic plot together with the absorption data of Fig. 9 for comparison. It is readily seen that two of the peaks of the photoionization cross-section spectrum agree with the main absorption lines within 0.2 meV. If the same assignment is tried for the spectrum of the photoionization cross section as for the absorption spectrum, this would imply a binding energy of 410.6 meV at 77 K for the ground state of the A center. This is indicated by the arrow F in Figs. 10 and 11. The good agreement between the binding energies obtained from absorption measurements at 5 K and from the spectrum of σ^0_{nA} at 77 K may suggest that the A center is pinned to the conduction band.

From EMT, it is known that the $2s$ state lies 35.3 meV (Ref. 4) below the conduction band. The corresponding peak in the spectrum of the photoionization cross section should therefore be seen at 375.3 meV. From investigations of shallow donors in silicon it is known that the $2sT_2$ state is somewhat deeper than predicted by EMT.[31] It is therefore not unreasonable to believe that the peak at 374.3 meV in Fig. 11 is caused by the absorption of electrons from the ground state into the $2sT_2$ state. A closer inspection of the absorption data shows that a weak line at the same energy is also observed in these measurements (Fig. 9).

The Arrhenius plot of the thermal emission rate for the A center e^t_{nA} (Fig. 5) gives a thermal activation energy of 364 meV which is equal to the sum E_2+E_a in the two-stage model. From lumines-

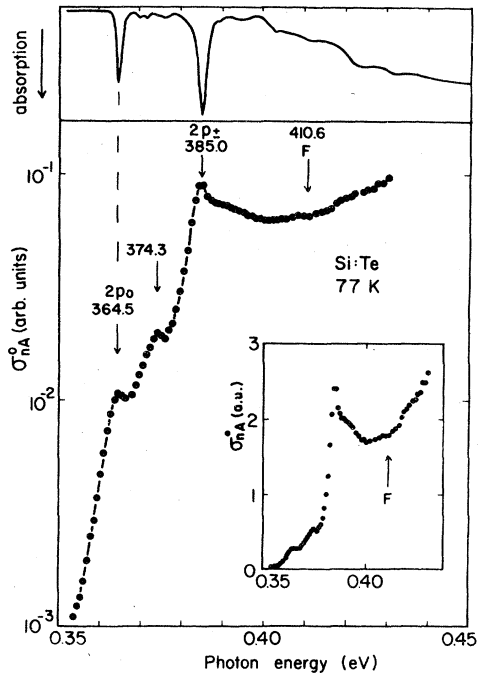

FIG. 11. Expanded version of the low-energy part of Fig. 10, plotted logarithmically in the main figure and linearly in the inset. The absorption data above the main figure are the same as in Fig. 9.

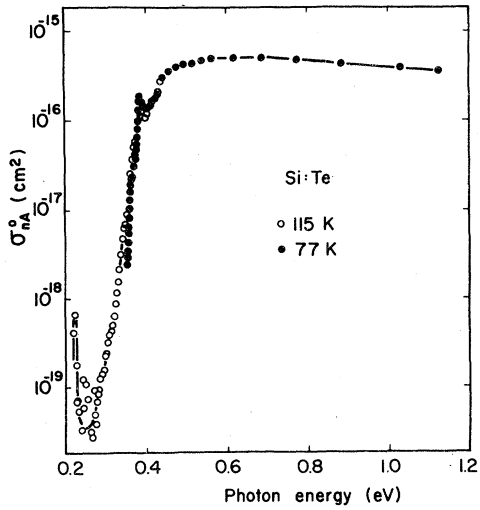

FIG. 12. Spectral dependence of the photionization cross section of electrons for the A center at 115 K (○), and 77 K (●). The sharp peak at about 0.23 eV in the 115-K spectrum is caused by the internal transition $1sA_1 \rightarrow 1sT_2$.

cence measurements, it is known[32] that the internal transition $2p_0 \rightarrow 1sA_1$ at least partly is radiative, and hence, it is not unreasonable to assume that E_a is zero. This would imply that the energy separation between the $1sA_1$ ground state and the $2p_0$ Rydberg state is given by the thermal activation energy of 364 meV. Hence, the value for the binding energy obtained from thermal measurements is in excellent agreement with the optical data shown in Figs. 9 and 11.

In Fig. 12 are shown spectra of the photoionization cross section σ^0_{nA} for two different temperatures. Compared with the spectrum taken at 77 K the corresponding peaks measured at 115 K are rather smeared out. However, in contrast to the 77-K spectrum, a sharp peak at about 0.23 eV is observed at 115 K. It is believed that this peak is caused by the internal transition $1sA_1 \rightarrow 1sT_2$ which is therefore strongly thermally activated. The energy position of the peak is in fair agreement with a corresponding line seen in absorption (cf. Fig. 6).

We tried to measure σ^0_{pA} by photocapacitance measurements. However, it turned out that the ratio $\sigma^0_{nA}/\sigma^0_{pA}$ was so large that no measurable change in occupancy could be achieved.[23] If no deeper centers are present in the sample such electronic properties are generally very favorable for the determination of σ^0_{pA} using the steady-state photocurrent technique.[23] From detailed investigations of photocurrent measurements, however, it was found that all our samples contained a residual midgap level with very large photoionization cross sections for both electrons and holes. Although the concentration of the midgap level was more than 2 orders of magnitude smaller than that of the A centers, the total photocurrent was nevertheless completely dominated by the midgap level.

In principle σ^0_{pA} can be studied by absorption measurements in p-type samples. Such samples were prepared by strongly counterdoping with boron. The diamagnetic charge state, Te^{2+}, and hence empty A centers, is stabilized by the Fermi level and infrared absorption from the photoionization process $Te^{2+} + h\nu \rightarrow Te^{+} + e^{+}$ may then result by exciting electrons from the valence band into empty A centers with an expected threshold energy of about 0.75 eV. This was indeed confirmed by measuring the spectral dependence of the Te^{+} ESR photoexcitation rate (see Sec. IV B). However, due to small values of σ^0_{pA} in this spectral region, infrared absorption was too weak to be detected directly. It is also noted here that no bound shallow excited states should exist because the holes are released optically from a Coulomb-repulsive Te^{+} core.

B. ESR measurements in Si:Te and Si:Se

Figure 13 shows the ESR spectrum of a tellurium-transported silicon crystal. The pattern is independent of the orientation of the magnetic field and is described by the spin Hamiltonian

$$\mathcal{H}=g_e\beta_e\vec{H}\cdot\vec{S}+a\vec{I}\cdot\vec{S}-g_n\beta_n\vec{H}\cdot\vec{I},\quad S=\tfrac{1}{2} \qquad (2)$$

where the first and last terms represent the electron and nuclear Zeeman interactions, respectively, and the second one the isotropic hyperfine (hf) coupling. The doublet splittings seen in Fig. 13 are consistent with the hf interaction of the $I=\frac{1}{2}$ nuclei of ^{123}Te and ^{125}Te. The hf couplings (see Table I) scale as their respective nuclear moments and the relative intensities of the lines correspond to the natural abundances of the Te isotopes. The strong central line arises from the even Te isotopes with zero nuclear spin. The centroids of the Te hf patterns are shifted from the position of this line by terms which are proportional to a^2/H. Table I lists the relevant ESR parameters.

The corresponding spectrum of selenium-diffused silicon is shown in Fig. 14. Here, the doublet is due to ^{77}Se ($I=\frac{1}{2}$). Table I compares the ESR data with those of Si:S$^+$.[33] As will be discussed below, the spectra presented in this paper are attributed to the ground states of the Te$^+$ and Se$^+$ donor levels, i.e., of the A centers in Si:Te and Si:Se.

Further resolution of the ESR lines of Si:Te$^+$ (Fig. 15) reveals a structure which can be attributed to the hf interaction of ^{29}Si ($I=\frac{1}{2}$ and 4.7% natural abundance) in the various shells surrounding Te. These would be described by the additional terms in the spin Hamiltonian:

$$\mathcal{H}(^{29}\mathrm{Si})=\sum_i\vec{S}\cdot T_i\cdot\vec{I}_i-g_n\beta_n\vec{H}\cdot\vec{I}_i, \qquad (3)$$

where i labels the quantities related to the ith surrounding nucleus. The Si hf pattern depends slightly on the orientation of the magnetic field H with respect to the crystal axes, since the tensors T_i are not isotropic. Their components are to be determined in an electron-nuclear double resonance (ENDOR) analysis.[34] In the lower part of Fig. 15, the intensities of the ^{29}Si lines are shown as obtained from a model assuming Te$^+$ to be located on a substitutional site. In this model, Te$^+$ has four neighbors in the first Si shell and twelve in the second one. The pattern obtained obviously resembles the structure of the ESR spectrum if the assignments of the lines are made as shown. For the orientation used ($\vec{H}||[100]$), the first-shell coupling is about 7.5 G. The corresponding value for Si:S$^+$ is 13.1 G.[33]

The present observations (large hf interactions with nuclei of Se and Te, isotropy of the resonances, small g shifts) are consistent with single unpaired electrons in s-type donor wave functions of Se$^+$ and Te$^+$. This assignment is also supported by the similarity of the spectra to those of Si:S$^+$.[33] It has been shown by Ludwig[33] that the electron spin S for this defect is indeed equal to $\frac{1}{2}$, which excludes sulfur on an interstitial site in the most likely $S=\frac{3}{2}$ electron configuration. However, a value of $\frac{1}{2}$ for S on an interstitial site cannot be ruled out. In the case of Te$^+$, our data and in particular the simulation of the ESR spectrum shown in the lower part of Fig. 15 may suggest that Te$^+$ in silicon should be on a substitutional site. For Te$^+$ on an interstitial site, the four first-shell neighbors have nearly the same distance (2.35 Å) to the donor ion as the six next-nearest ones (2.70 Å). Assuming a similar hf coupling for both types of ions, one expects a total multiplicity of 10 for these closest ions instead of four in the substitutional model. The lines assigned to the first shell in Fig. 15 should thus be about 2.5 times higher for an interstitial Te. The number of ions in the next possible positions is twelve for both choices of donor positions.

A final assignment of the donor position is expected from a reconstruction of the ESR spectrum from the ^{29}Si hf interactions obtained from an EN-

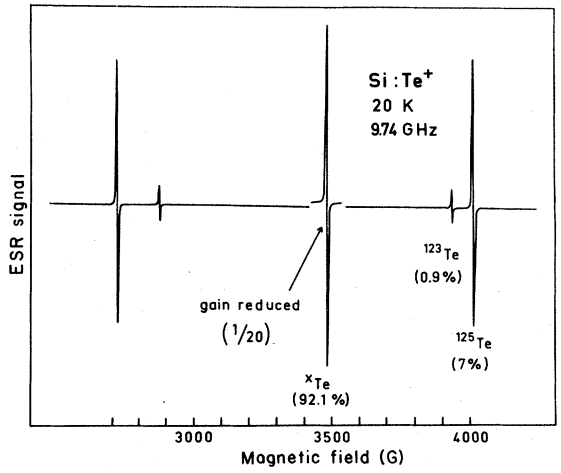

FIG. 13. ESR of the ground state of the Te$^+$ donor in silicon. The doublets arise from the Te isotopes indicated. Their natural abundancies are also given. ^{x}Te denotes even Te isotopes with zero nuclear spin.

TABLE I. ESR parameters of S^+, Se^+, and Te^+ donor ground states in silicon. The values in parentheses signify the uncertainties of the measurements in units of the last figure shown. All isotopes of S, Se, and Te have the same g value.

	g	$\|a\|$ $(10^{-4}\ cm^{-1})$	Reference
$^{33}S^+$	2.0054 (2)	104.2 (2)	33
$^{77}Se^+$	2.0057 (3)	553.2 (2)	present work
$^{125}Te^+$	2.0023 (2)	1164.7 (2)	present work
$^{123}Te^+$	2.0023 (2)	966.1 (2)	present work

DOR analysis and from the line intensities corresponding to the probabilities of finding ^{29}Si in the shells surrounding Te^+.

For the chalcogen donor wave functions, g is expected to be close to that of a free electron, as has been observed for Te^+. Small positive deviations have, however, been found for Se^+ and S^+. These deviations can be attributed to the admixture of states corresponding to holes in the valence band to the donor wave function induced by the local Si spin-orbit coupling.[35] Such contributions are expected to become smaller with increasing distance of the donor level from the valence band. The g shift is therefore smaller for Te^+ than for S^+ and Se^+. There is apparently no influence of the spin-orbit coupling of the donor ions themselves, as indicated by the similarity of the g values of Se^+ and S^+ in spite of the large difference in spin-orbit coupling.

The hf interactions of the chalcogen nuclei lead to estimates of the probabilities of finding the unpaired electrons near the donor ions. In Table II the spin densities $|\Psi(0)|^2$ at the respective nuclei, as determined from $a = 8\pi/3 g_e \beta_e g_n \beta_n |\Psi(0)|^2$, are compared with values expected for ns states in the $(ns)^2(np)^3$ electron configuration of the free S^+, Se^+, and Te^+ ions. These values have been calculated from Hartree-Fock wave functions of the free ions.[36] It is readily seen that the density of the unpaired electrons is about 10% at the central ions of the donor centers in all three cases. Hartree-Fock calculations of the contact hf interaction in s-state ions, however, generally underestimate the actual interactions, since they are not able to take proper account of the correlations with inner-shell electrons. Corrections to include such effects were ob-

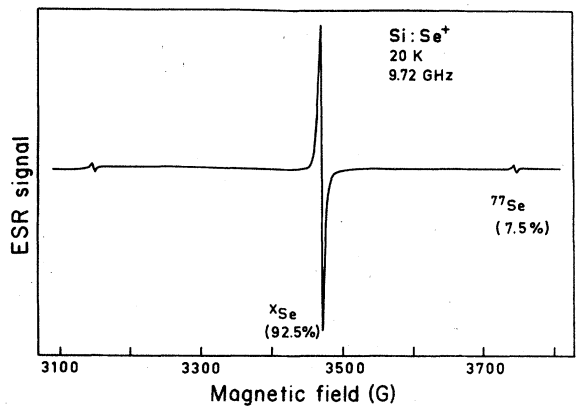

FIG. 14. ESR of the ground state of the Se^+ donor in silicon.

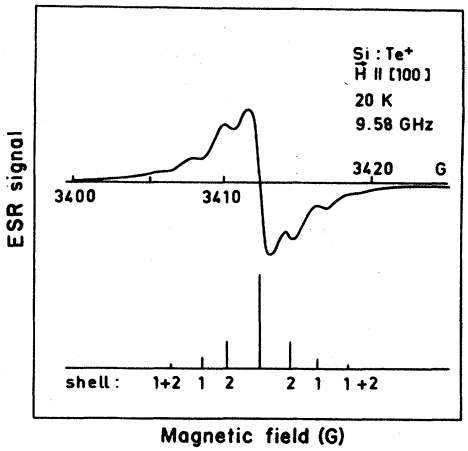

FIG. 15. High-resolution ESR spectrum of the central line of Fig. 13. The structure lying symmetrically with respect to the main line is due to hyperfine interactions with ^{29}Si nuclei surrounding Te^+. The diagram in the lower part of the figure presents a possible assignment of the lines assuming substitutional Te. The intensities correspond to the probabilities of finding ^{29}Si in the shells indicated.

TABLE II. Spin densities of S^+, Se^+, and Te^+ donor ground states at the donor nuclei. Values of $|\Psi(0)|^2$ in the first column are experimental. In the second column these have been divided by the Hartree-Fock prediction for the free atom (FA), i.e., the density of the *ns* part in the $(ns)^2(np)^3$ state of S^+, Se^+, Te^+ at the respective nucleus. In the third column, the atomic values have been corrected via Goudsmit's formula (see Table III). The data are otherwise as in the second column.

	$\lvert\Psi(0)\rvert^2$ (10^{24} cm^{-3})	Ψ^2/Ψ^2_{FA}	Ψ^2/Ψ^2_{FA}
S^+	6.13	0.106	0.094
Se^+	13.18	0.115	0.103
Te^+	16.65	0.119	0.110

tained by comparison with densities resulting from the semiempirical Goudsmit formula. The method is indicated in Table III which lists the free-ion predictions used in the analysis given in Table II. It is clear from Table II that even if the mentioned corrections are included, the densities of the unpaired electrons at the donor ions remain about 10%.

Turning to the ^{29}Si hf interaction, it should be noted that the couplings with the Si shell closest to the donor are larger in the case of S^+ than for Te^+. One has to conclude that the donor wave function for Si:Te^+ is less compact and approaches more a conduction-band state. This is consistent with the smaller energy distance from the conduction-band edge of this donor. A thorough discussion of this point has, however, to await the results of an ENDOR analysis of Si:Te^+.[34]

Some insight into the chalcogen donor wave functions can nevertheless be obtained from ^{29}Si ENDOR data of Si:S^+ which are already available.[33,37] For the nearest-neighbor Si ligands, the tensor T_i is axially symmetric around the bond direction with $T_{||} = -20.2$ G and $T_\perp = -7.4$ G. The isotropic part a is thus -11.7 G and the anisotropic one b is -4.3 G. Comparing these values with those expected for the Si free atom 3*s* and 3*p* wave functions, a_f and b_f,[37] respectively, one finds $a/a_f = 0.008$ and $b/b_f = 0.12$. The donor electron is thus found at each of the Si ligands with a probability of about 13% and moves there in essentially a *p*-type orbital pointing towards the S^+ site. The hf interactions with S ($\sim 10\%$) and its four first-shell ligands [$4\times(13\%)$] can thus account for about 60% of the spin density of the unpaired electron, emphasizing the rather small radius of the wave function of this deep donor. It should be noted that the density is higher at the ligand than at the donor core, in contrast to the situation in an effective-mass orbital. This finding appears to be the first experimental demonstration of the fact that the unpaired electron rather moves in an antibonding orbital[38] orthogonal to a binding state deep in the valence band. For this latter state, the highest density is expected at the donor core. Hence, in the orthogonal, antibonding orbital, the density must move out to the ligands, as is actually observed.

TABLE III. Predictions for spin densities for free S^+, Se^+, and Te^+ ions at the nuclei. In the first column, the Hartree-Fock (HF) values are calculated from functions tabulated in Ref. 35. In the second column, the HF values are corrected by factors obtained by comparing the free-ion Hartree-Fock predictions for the alkali-like series S^{5+}, Se^{5+}, and Te^{5+} (see Ref. 44) with values calculated from the semiempirical Goudsmit formula (see Refs. 45–47).

	$\lvert\Psi_{ns}(0)\rvert^2$ (10^{24} cm^{-3})	$\lvert\Psi_{ns}(0)\rvert^2$ (10^{24} cm^{-3})
S^+	57.9	66.0
Se^+	114.2	127.9
Te^+	139.5	182.8

Photon-induced valency changes of Te^+ and Te^{2+} were investigated in two samples with different positions of the Fermi level.[39] One was *n*-type with a room-temperature resistivity of about 1.7 Ω cm and the other *p*-type with a resistivity of about 1 Ω cm. For the *n*-type samples the ESR signal was very strong, indicating that the Fermi level was above the *A* center. In the *p*-type material, only a weak Te^+ signal was observed when the sample was cooled to 20 K in the dark. The Te^+ signal could be reduced to zero by illuminating the sample with photons of energy less than 0.7 eV but larger than 0.4 eV. Most of the measurements to study the spectral energy dependence of the creation and quenching of Te^+ by illumination with light were performed on this *p*-type specimen, although quenching of Te^+ was also observed with the *n*-type sample. These measurements provide strong evidence that the microscopic models for Si:Te^+ and Si:Se^+ suggested in this paper are indeed responsible for the relevant optical and photocapacitance features studied.

Figure 16 shows schematically the time dependence of the Te^+ signal, i.e., the concentration of filled *A* centers in the *p*-type sample due to illumination. When the sample was illuminated

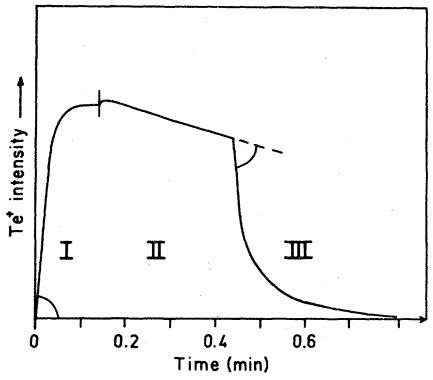

FIG. 16. Schematic time dependence of the photoresponse of Te^+ in p-type Si. I: excitation with $h\nu \geq E_c - E_T$; II: light off; III; quenching with $h\nu \geq E_T$.

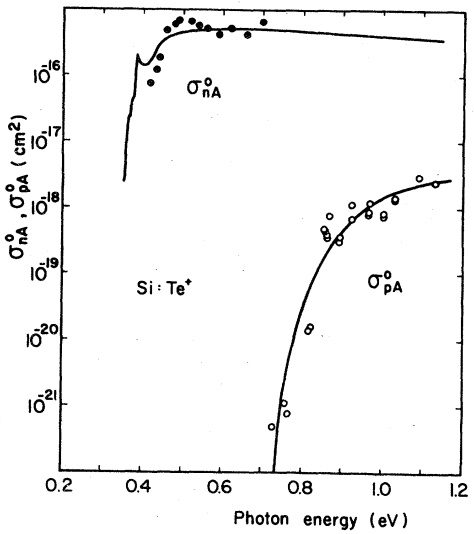

FIG. 17. Energy dependence of the photoionization cross sections of Si:Te^+ for holes, σ^0_{pA} (○), and electrons σ^0_{nA} (●), as determined by ESR. The vertical scales for both quantities are based on different calibrations, as described in text. The solid curve in the σ^0_{nA} spectrum is a plot of the photocapacitance data shown in Fig. 10. The absolute values of the σ^0_{nA} data obtained by ESR are adjusted to give optimal agreement with photocapacitance data. The adjustment is within the experimental error. It should be noted that the photocapacitance data for energies smaller than about 0.4 eV are due to photothermal excitation processes and therefore thermally activated. At low temperatures these excitation processes are thus not observed, in agreement with the ESR data shown.

with photons of a particular energy specified below, Te^+ was created (I). It should be noted that the initial conditions were chosen to be such that all A centers were empty and hence the initial Te^+ concentration $n_T(0)$ was zero. After removing the light source, the Te^+ intensity first increased slightly and then decreased slowly (II). Illumination of the sample with photons of another energy during this stage led to a strong decrease in the Te^+ signal (III). The slopes defined in Fig. 16 were taken as a measure of the sensitivity of the system to light irradiation.

Figure 17 shows the generation and annihilation of Te^+ centers (filled A centers) in silicon as a function of photon energy. It is easily seen that the A centers start to fill at about 0.73 eV, in good agreement with the energy position of the centers obtained from junction space-charge techniques and absorption measurement (Figs. 9 and 10). The rate of filling is given by $\sigma^0_{pA}\phi N_{TT}$ where N_{TT} is the total concentration of A centers. Reflection at the crystal surface has been taken into account in determing ϕ. Assuming that tellurium forms only single substitutional impurity centers, N_{TT} has been determined to be about 1×10^{17} cm^{-3} from mass spectrometric analysis.[40] The absolute values of σ^0_{pA} are taken to be correct within a factor of 5.

The light-induced quenching of the Te^+ signal is obviously caused by the optical excitation of electrons from filled A centers into the conduction band. The rate of the quenching process is given by $\sigma^0_{nA}\phi n_T(0)$. The spectral distribution of the photoionization cross section of electrons σ^0_{nA} is shown in Fig. 17 together with the data obtained from photocapacitance measurements at 77 K (cf. Fig. 12). Since $n_T(0)$ has been measured by comparison with a Si:P^0 ESR standard,[41] absolute σ^0_{nA} values are directly obtained from the quenching rate.

The increase of the Te^+ signal after removing the light source (II in Fig. 16) can be understood as follows: The generation of Te^+ and, hence, the filling of empty A centers in a steady state is stabilized by recombination of electrons from the A centers with holes in the valence band and further optical excitation of electrons from the A center into the conduction band. Electrons excited to the conduction band may be recaptured by trapping centers, possibly empty B centers. The increase in the Te^+ intensity may therefore be caused by the reverse process. After the slight initial increase the decrease of the Te^+ signal in darkness (II in Fig. 16) is known from our photocapacitance measurements, to be due to room-temperature radiation causing photothermal excitation of electrons from the ground state into the conduction band via the Rydberg series.

These results were confirmed by measurements on the *n*-type Si:Te sample. By comparing the Te concentration obtained from mass spectrometric analysis with the Te^+ concentration determined with ESR, it turned out that the number of filled *B* centers was negligibly small. Changes of the Te^+ signal were observed only with photons of energy large enough to excite electrons from the *A* centers to the conduction band. From the initial slopes of the Te^+ quenching, values in good agreement with the data obtained with the *p*-type sample were derived. After removing the light source, the Te^+ signal returned to its initial dark value within a few seconds at 20 K.

A study of the photoionization cross section in Si:Se is shown in Fig. 18. Since the *A* center in Si:Se is a midgap level and the concentration of filled *A* centers in thermal equilibrium was much larger than in our Si:Te samples, the measurements were more difficult to perform than in the case of tellurium. Nevertheless, the extent to which the initial Se^+ signal (i.e., the concentration filled *A* centers) could be reduced by illuminating the sample with photons of energy of about 0.6 eV was large enough to observe net effects which were in agreement with the data obtained from previous measurements of photocapacitance[8] (the solid lines in Fig. 18). Hence, these results also make possible an interpretation of previous experimental data in Si:Se on the microscopic basis.

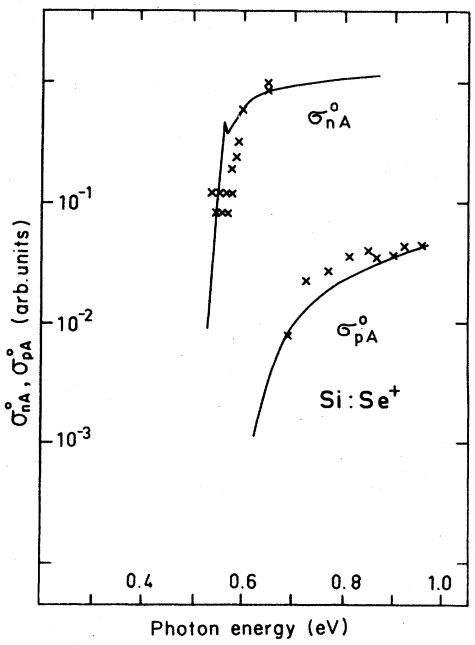

FIG. 18. Energy dependence of the photoionization cross sections of $Si:Se^+$, as determined by ESR. The vertical scales of the experimental data have been adjusted to give optimal coincidence with the photocapacitance data (solid lines) reported in Ref. 8.

V. DISCUSSION

As in the case of Si:S (Ref. 6) and Si:Se (Ref. 7), two dominant donor levels are observed when tellurium is incorporated in silicon at 1200 °C. The spectra of electron transitions from the chalcogen donor levels to the conduction band are best understood in terms of excited states. Two types of excited states are involved. Those which are generally referred to as the Rydberg series are in good agreement with calculated values of singly and doubly charged centers using EMT.[4] Hence, the ground-state binding energies of all chalcogen donors could be determined with high accuracy (Table IV). The highest energy resolution was obtained in Si:Te, resulting in data of an accuracy, which to the best of our knowledge, has hitherto not been obtainable in deep-level spectroscopy.

TABLE IV. Excitation energies (meV) for chalcogens in silicon relative to the ground-state. S^0 values are taken from photoconductivity measurements in Ref. 49, S^+ (and Se^+) values are from photocapacitance measurements in Ref. 8 (although the designations of the peaks are different). The Se values are taken from the absorption measurements in Ref. 48 and the Te data from the present work.

	S^0	S^+	Se^0	Se^+	Te^0	Te^+
$1sT_2$	283	428	272	428	160	234
$2p_0$	307	567	295	544	187	364
$2p_\pm$	312	586	300	564	192	385
conduction band	318	612	307	589	199	411

In agreement with previous investigations, our ESR measurements clearly show that the donor levels studied in Si:Se and Si:Te by junction space-charge techniques and absorption measurements are all chalcogen-related centers. Furthermore, the interpretation of our ESR results, together with the thermal and optical data presented in this paper, suggests that tellurium forms isolated substitutional impurity centers in silicon. Since the properties of Si:S and Si:Se are similar to those of Si:Te, it is probable that also in these cases the properties of substitutional double donors have been studied. The donor levels investigated are then the neutral D^0 (B centers) and singly ionized D^+ (A centers) charge states of the corresponding substitutional double donors.

As pointed out earlier, multivalley splitting is only expected when the donor wave function is built up mainly from conduction-band states. That this is valid for all chalcogen donor levels has been confirmed by the observation of split-off levels and is further supported by the facts that the g values of the A centers are very close to that of free electrons and that, in all cases studied, the ground-state binding energies are independent of temperature (which means that the chalcogen donor levels are probably pinned to the conduction band).

EMT is in good agreement with experimental results obtained for excited states such as Rydberg series, but has had limited success for the ground states even for shallow levels. In Fig. 19, the experimentally observed energy states of the chalcogen donor levels are compared with the corresponding EMT values and helium states. It is quite evident that for all chalcogens the multivalley split-off $1s$ state is deeper than expected from EMT. Among the excited states, the deviation is largest for the $1sT_2$ states of Te^+ and S^+ which lie about 0.18 eV below the conduction-band edge instead of 125 meV as derived from EMT. On the other hand, only slightly larger values were found for the $1sT_2$ states of S^0 and Se^0. For these centers, the $1sT_2$ states were rather close to a value of about 34 meV which is observed for shallow donors[26] (cf. Table IV). Furthermore, it is easily seen that the $1sA_1$ ground states of the neutral B centers are in all cases much deeper than the corresponding ground states of the singly charged A centers after correction for effective charge. A similar behavior is found for the He system. If the effective charges Z of the cores of the neutral donors were exactly equal to 1 in all cases, their $1sA_1$ ground states would have the same binding energy as the singly-ionized donors[42] in the scheme used in Fig. 19, where corrections are made for different charge states. As for He^0, the deviation from $Z=1$ is obviously caused by electron-electron correlations which prevent spherically symmetric screening of the twofold core charge by electron 1. Electron 2 thus experiences an effective charge $1<Z<2$. As can be seen from Fig. 19, an appreciable part of the ground-state energy of the neutral donors is due to this mechanism. This can at least partly explain why compared to the shallow donors P^0, As^0, and Sb^0, these neutral donors are so deep. It should be noted that such correlation effects are much weaker for the excited states, since the electron-electron interaction is strongly reduced,

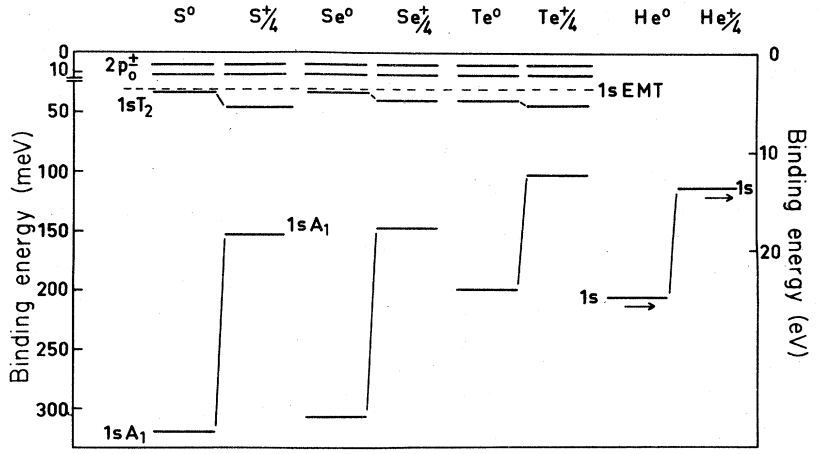

FIG. 19. A comparison of the energy-level schemes for chalcogens in silicon and the helium atom. For energy values and references, see Table IV.

because of the larger orbital radii.

In a forthcoming paper,[43] we intend to discuss in detail the chemical thermodynamics of the chalcogen transport systems, the different properties of the resulting products, and to compare them with data from chalcogen-diffused specimens. A model of the chemical bond situation for *all* chalcogens in silicon will also be presented.

Note added

A different interpretation of the two peaks at 234.2 and 239.6 meV in Fig. 6, upper curve, is given in a forthcoming paper by H. G. Grimmeiss, E. Janzén, and K. Larsson. The authors ascribe the doublet to transitions from the ground state $1sA_1$ to spin-orbital split $1sT_2$ states.

Recently A. L. Lin, A. G. Crouse, J. Wendt, A. G. Campbell, and R. Newman [Appl. Phys. Lett. 38, 683 (1981)] investigated the electrical and optical properties of a neutral tellurium center. The binding energy reported is identical with that of the *B* level in this paper.

ACKNOWLEDGMENTS

We thank Dr. U. Kaufmann, Dr. J. R. Niklas, and Professor J. M. Spaeth for valuable discussions and helpful comments. The experimental assistance of Mr. K. Sambeth and Mr. M. Schlabach is gratefully acknowledged. We also greatly appreciate the support of Dr. C. Solbrig and Mr. A. Breitschwerdt.

[1]W. Kohn, in *Solid State Physics,* edited by F. Seitz and D. Turnbull (Academic, New York, 1957), Vol. 5, p. 257.
[2]W. Kohn, Phys. Rev. 98, 915 (1955).
[3]S. T. Pantelides, Rev. Mod. Phys. 50, 797 (1978).
[4]R. A. Faulkner, Phys. Rev. 184, 713 (1969).
[5]A. Glodeanu, Phys. Status Solidi 19, K43 (1967).
[6]H. G. Grimmeiss, E. Janzén, and B. Skarstam, J. Appl. Phys. 51, 3740 (1980).
[7]H. G. Grimmeiss, E. Janzén, and B. Skarstam, J. Appl. Phys. 51, 4212 (1980).
[8]H. G. Grimmeiss and B. Skarstam, Phys. Rev. B 23, 1947 (1981).
[9]S. D. Brotherton, M. J. King, and G. J. Parker, J. Appl. Phys. (in press).
[10]A. S. Lyutovich, V. P. Prutkin, V. M. Mikhaelyan, D. S. Gafitulina, and Z. V. Abramova, Fiz. Tekh. Poluprovodn. 2, 878 (1968) [Sov. Phys.—Semicond. 2, 728 (1968)].
[11]N. S. Zhdanovich and Y. I. Kozlov, Fiz Tekh. Poluprovodn. 9, 1594 (1975) [Sov. Phys.—Semicond. 9, 1049 (1976).
[12]T. F. Lee, R. D. Pashley, T. C. McGill, and J. W. Mayer, J. Appl. Phys. 46, 381 (1975).
[13]S. T. Picraux, N. G. E. Johansson, and J. W. Mayer, in *Semiconductor Silicon,* edited by R. R. Haberecht and E. L. Kern, (Electrochemical Society, New York, 1969). p. 422.
[14]O. Meyer, N. G. E. Johnansson, S. T. Picraux, and J. W. Mayer, Solid State Commun. 8, 529 (1970).
[15]J. Gyulai, O. Meyer, R. D. Pashley, and J. W. Mayer, Radiat. Eff. 7, 17 (1971).
[16]G. Foti, S. U. Campisano, E. Rimini, and G. Vitali, J. Appl. Phys. 49 2569 (1978).
[17]A. Nylandsted Larsen, G. Weyer, and L. Nanver, Phys. Rev. B 21, 4951 (1980).
[18]S. Fischler, *Metallurgy of Advanced Electronics Materials* (Interscience, New York, 1963),Vol. 19, p. 273.
[19]H. G. Grimmeiss, E. Janzén, B. Skarstam, and A. Lodding, J. Appl. Phys. 15, 6238 (1980).
[20]E. Sirtl, J. Phys. Chem. Solids 24, 1285 (1963),
[21]F. H. Nicoll, J. Electrochem. Soc. 110, 1165 (1963).
[22]C. Holm and E. Sirtl, J. Cryst. Growth 54, 253 (1981).
[23]H. G. Grimmeiss and C. Ovrén J. Phys. E (in press).
[24]J. A. Pals, Solid-State Electron. 17, 1139 (1974).
[25]H. G. Grimmeiss, Ann. Rev. Mater, Sci. 7, 341 (1977).
[26]R. L. Aggarwal and A. K. Ramdas, Phys. Rev. 140, A1246 (1965).
[27]R. M. Gibb, G. J. Rees, B. W. Thomas, B. L. H. Wilson, B. Hamilton, D. R. Wight, and N. F. Mott, Philos. Mag. 36, 1021 (1977).
[28]D. V. Lang, J. Appl. Phys. 45, 3014 (1974); 45, 3023 (1974).
[29]D. R. Bosomworth, W. Hayes, A. R. L. Spray, and G. D. Watkins, Proc. Soc. London Ser. A 317, 133 (1970).
[30]K. Krishnan (unpublished).
[31]H. J. Hrostowski and R. H. Kaiser, J. Phys. Chem. Solids 7, 286 (1958).
[32]J. Weber (private communication).
[33]G. W. Ludwig, Phys. Rev. 137 A1520 (1965).
[34]J. M. Spaeth (private communication).
[35]In, e.g., Si:S^+ the density of the unpaired electron is to a large extent localized within and on the first-shell ions. At the first-shell ions, the electron has mainly *p* character. Close to these silicon atoms, the wave function is therefore similar to that of the Si *E* center for which a Δg mechanism similar to the one sketched here, has been suggested (see Ref. 47). The Si *E* center is one of the dominant defects produced by

electron irradiation in phosphorous-doped vacuum floating-zone silicon.
[36]E. Clementi and C. Roetti, At. Data Nucl. Data Tables 14, 177 (1974).
[37]For the following evaluation see, e.g., G. D. Watkins, in *Point Defects in Solids,* edited by J. H. Crawford, and L. M. Slifkin (Plenum, New York, 1975), Vol. 2, p. 348.
[38]H. P. Hjalmarson, P. Vogl, D. J. Wolford, and J. D. Dow, Phys. Rev. Lett. 44, 810 (1980).
[39]For an earlier application of this method see, e.g., K. W. Blazey, O. F. Schirmer, W. Berlinger, and K. A. Müller, Solid State Commun. 16, 589 (1975).
[40]A. Hurrle (private communication).
[41]It was found that Te^+ concentrations formed by photoexcitation were generally 1 order-of-magnitude smaller than that determined by mass spectrometry. At high-excitation intensities, Te^+ concentrations increased nonlinearly with photon flux.
[42]The non-Coulombic, central cell part of the potential is not considered in this argument.
[43]C. Holm and E. Sirtl, J. Electrochem. Soc. (in press).
[44]S. Fraga, and J. Karwowski, K. M. S. Saxena, *Handbook of Atomic Data,* (Elsevier, Amsterdam, 1976).
[45]S. Goudsmit, Phys. Rev. 43, 636 (1933).
[46]W. Kohn and J. M. Luttinger, Phys. Rev. 97, 883 (1961).
[47]G. D. Watkins and J. W. Corbett, Phys. Rev. 134, A1359 (1964).
[48]J. C. Swartz, D. H. Lemmon, and R. N. Thomas, Solid State Commun. 36 331 (1980).
[49]R. G. Humphreys and P. Migliorato (unpublished).